Qubit Architecture with High Coherence and Fast Tunable Coupling

Yu Chen,[1,†] C. Neill,[1] P. Roushan,[1,†] N. Leung,[1] M. Fang,[1] R. Barends,[1,†] J. Kelly,[1] B. Campbell,[1] Z. Chen,[1] B. Chiaro,[1] A. Dunsworth,[1] E. Jeffrey,[1,†] A. Megrant,[1,2] J. Y. Mutus,[1,†] P. J. J. O'Malley,[1] C. M. Quintana,[1] D. Sank,[1,†] A. Vainsencher,[1] J. Wenner,[1] T. C. White,[1] Michael R. Geller,[3] A. N. Cleland,[1] and John M. Martinis[1,*,†]

[1]*Department of Physics, University of California, Santa Barbara, California 93106-9530, USA*

[2]*Department of Materials, University of California, Santa Barbara, California 93106-5050, USA*

[3]*Department of Physics and Astronomy, University of Georgia, Athens, Georgia 30602, USA*

(Received 14 March 2014; published 26 November 2014)

We introduce a superconducting qubit architecture that combines high-coherence qubits and tunable qubit-qubit coupling. With the ability to set the coupling to zero, we demonstrate that this architecture is protected from the frequency crowding problems that arise from fixed coupling. More importantly, the coupling can be tuned dynamically with nanosecond resolution, making this architecture a versatile platform with applications ranging from quantum logic gates to quantum simulation. We illustrate the advantages of dynamical coupling by implementing a novel adiabatic CONTROLLED-Z gate, with a speed approaching that of single-qubit gates. Integrating coherence and scalable control, the introduced qubit architecture provides a promising path towards large-scale quantum computation and simulation.

DOI: 10.1103/PhysRevLett.113.220502 PACS numbers: 03.67.Lx, 85.25.Cp, 85.25.Hv

The fundamental challenge for quantum computation and simulation is to construct a large-scale network of highly connected coherent qubits [1,2]. Superconducting qubits use macroscopic circuits to process quantum information and are a promising candidate towards this end [3]. Recent materials research and circuit optimization have produced significant progress in qubit coherence [4–6]. Superconducting qubits can now perform hundreds of operations within their coherence times, allowing the development of complex algorithms [7–9].

It is desirable to combine these high-coherence qubits with tunable interqubit coupling; the resulting architecture would allow both coherent local operations and dynamically varying qubit interactions. For quantum simulation, this would provide a unique opportunity to investigate dynamic processes in nonequilibrium phenomena [10–15]. For quantum computation, such an architecture would provide isolation for single-qubit gates yet enable fast multiqubit gates that minimize decoherence errors.

Despite previous successful demonstrations [16–26], these applications have yet to be realized due to the challenge of implementing tunable coupling without degrading the device performance. Serious control cross talk arises when there is a dc path connecting the qubit and coupler junctions [16–21]. Furthermore, the coupler circuit can introduce additional decay channels through which the qubit decoheres [17].

Here, we introduce a qubit architecture that incorporates fast tunable coupling, high coherence, and minimal cross talk. In contrast to previous designs, our "gmon" device inductively couples transmon qubits at their low voltage node. This design strategy substantially reduces the qubit energy stored in the coupler, minimizing the influence of added loss and retaining the coherence of the transmon. In addition, it eliminates all dc connectivity between the qubit and the coupler junctions, dramatically reducing the control cross talk of the circuit. With the coupling turned off, we demonstrate that our architecture is protected from the frequency crowding problems that arise from fixed coupling. By dynamically tuning the coupling, we implement a novel adiabatic CONTROLLED-Z (CZ) gate at a speed approaching that of single-qubit gates.

A two-qubit unit cell with tunable coupling is shown in Fig. 1(a). The qubits and control lines are defined by an aluminum film with cuts exposing the underlying sapphire substrate. Our circuit design is based on the Xmon qubit [5], consisting of a cross-shaped capacitor resonating with a nonlinear inductor $L_J = 9.0$ nH from a dc SQUID. We modify the Xmon design to introduce a linear inductor $L_g = 200$ pH from the junction to ground, with $L_g \ll L_J$, so the qubit nonlinearity is largely unaffected [27]. This inductor introduces a node where current from one qubit can be tapped off to interact with a neighboring qubit. A junction connecting the two nodes provides a tunable inductance L_c that controls the flow of this current and therefore the coupling.

The physics behind this tunable coupler is well explained using a simple linear model, since the coupling currents are much smaller than the critical current of the coupling junction $I_0 = 330$ nA; see Ref. [32] for a full quantum mechanical treatment. A circuit diagram for the device is given in Fig. 1(b). An excitation current I_q in the first qubit mostly flows through L_g, with a small fraction $I_{\rm cp} = I_q L_g/(2L_g + L_c)$ flowing through the coupler to the second qubit. This current generates a flux in the second qubit $\Phi_2 = L_g I_{\rm cp}$. Ignoring parasitic inductance, the effective mutual inductance can be expressed as

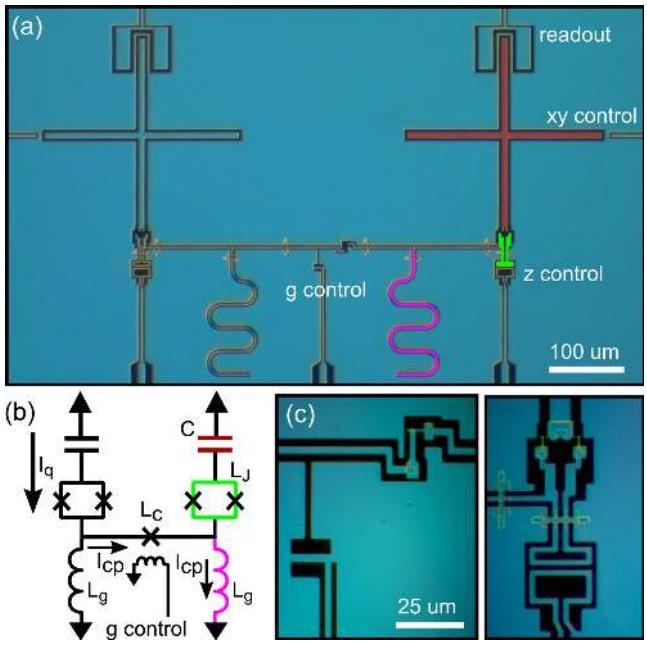

FIG. 1 (color online). (a) Optical micrograph of two inductively coupled gmon qubits. The cross-shaped capacitors are placed in series with a tunable Josephson junction and followed by a linear inductor to ground. The circuit is depicted schematically in (b) with arrows indicating the flow of current for an excitation in the left qubit. The qubits are connected with a junction serving as a tunable inductor to control the coupling strength. (c) Micrographs of the coupler junction (left) and qubit SQUID (right). The bottom of each image shows a bias line to adjust the coupling strength (left) and qubit frequency (right, not shown in schematic).

$$M = \frac{\Phi_2}{I_q} = \frac{L_g^2}{2L_g + L_c}. \tag{1}$$

Using this mutual inductance, the interaction Hamiltonian for the two qubits on resonance is

$$\hat{H}_{\text{int}} = -\frac{\omega_0}{2}\frac{M}{L_J + L_g}(\hat{a}_1^\dagger \hat{a}_2 + \hat{a}_1 \hat{a}_2^\dagger), \tag{2}$$

where ω_0 is the qubit resonance frequency. This equation uses the rotating wave approximation to express photon swapping with raising and lowering operators [26]. The coefficient of the interaction Hamiltonian gives the coupling strength

$$g = -\frac{\omega_0}{2}\frac{L_g}{L_J + L_g}\frac{L_g}{2L_g + L_{c0}/\cos\delta}, \tag{3}$$

where we replaced L_c by the Josephson inductance $L_c = \Phi_0/(2\pi I_0 \cos\delta) \equiv L_{c0}/\cos\delta$. Here, δ is the phase difference across the coupler junction, set by applying a dc flux. The coupling g can be varied continuously from negative to positive, going smoothly through zero at $\delta = \pi/2$. This smooth transition ensures the existence of a bias where the coupling is completely negated, even with small stray coupling.

A critical part of our design is its compatibility with high coherence. The key concept to maintain coherence is the voltage divider created by L_J and L_g. Placing the coupling circuit at this low voltage node reduces capacitive losses to surface defects on coupler structure by a factor of $(L_J/L_g)^2$—over 2000 in our design. For the gmon, we measure an energy relaxation time $T_1 \sim 7$–10 μs, independent of the coupling strength (see Ref. [27]). This is comparable to that of Xmon devices with similar capacitor geometry (8 μm center trace, 4 μm gap) and aluminum deposition conditions (high vacuum e-beam evaporation). Devices grown with molecular beam epitaxy and with optimized capacitor geometry have demonstrated lifetimes exceeding 40 μs [5].

In addition to the energy dissipation, the coupler circuit may introduce additional dephasing to the qubits. In order to minimize dephasing, we have designed the gmon circuit in a way that the qubit frequency has a weak dependence on the coupler bias, only a few tens of MHz per flux quantum. Near the optimal bias point, we have measured a dephasing time T_φ of 3–4 μs, over the entire range of coupling strength from zero to its maximum value [27]. This is comparable to that of the Xmon qubit, indicating that the dephasing rate of the qubit is unaffected by the coupler circuit.

The core functionality of the gmon coupler is demonstrated in Fig. 2. In Fig. 2(a) we show the variation of coupling strength as a function of the coupler flux bias when the two qubits are brought into resonance at frequency $\omega_0/2\pi = 5.67$ GHz. Here, for one qubit we sweep the microwave drive frequency and measure the qubit excited state probability P_1. We observe two distinct resonances at frequencies $\omega_0 + g$ and $\omega_0 - g$, resulting from the coupling-induced energy level splitting. The total splitting is twice the coupling strength, ranging from 0 to 110 MHz. This range can be further increased by modifying the coupler junction critical current. Note that we have compensated for the small changes in the qubit frequency ($\sim g$) that occur as L_c is varied. These compensations are small because dc control currents flow only through the coupler and not through the qubit junctions as the qubit capacitor acts as a dc block. Reference [27] gives details on how the qubit and coupler controls are effectively made orthogonal.

In Fig. 2(b), we set the the coupling strength to its maximum value and rapidly exchange an excitation between the two qubits. We excite the first qubit (Q_1), turn on the coupling, wait a variable delay time, and then measure the excited state probability of Q_1. We vary the frequency of Q_1 while fixing that of the second qubit (Q_2). The interaction produces the expected chevron pattern [33]. The strong coupling allows the excitation to swap between

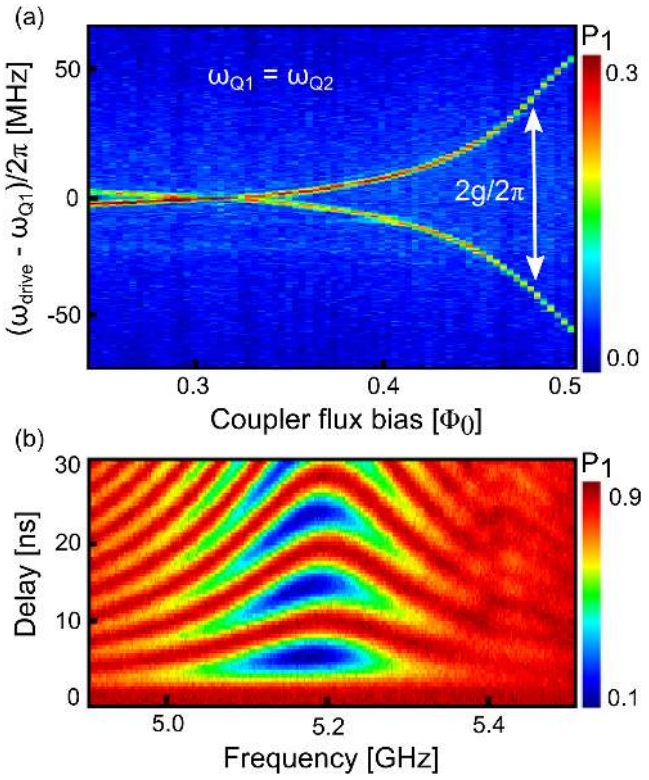

FIG. 2 (color online). (a) The dependence of coupling strength on the coupler flux bias while the two qubits are on resonance, with $\omega_{Q1}/2\pi = \omega_{Q2}/2\pi = 5.67$ GHz. For each value of the coupler flux bias, we sweep the microwave drive frequency and measure the excited state probability P_1 (color bar) of Q_1. There are two distinct peaks in the spectroscopy resulting from the qubit energy level splitting. The frequency splitting is twice the coupling strength $g/2\pi$ and ranges from 0 to 110 MHz. (b) Q_1 excited state probability (color bar) versus Q_1 frequency (horizontal axis) after exciting Q_1 and waiting a variable delay time (vertical axis). Q_2 is fixed at 5.18 GHz and the coupling set to 55 MHz. On resonance, the two qubits swap an excitation in 5 ns.

the qubits in 5 ns, consistent with the 110 MHz splitting measured above. At this rate, a $\sqrt{i\mathrm{SWAP}}$ gate could generate a Bell state in 2.5 ns, whereas a nonadiabatic CZ could be implemented in 10 ns [34]. We have also performed the same measurement with nominally zero coupling (see Ref. [27]) and observe no indication of swapping after 6 μs. This places an upper bound on the residual coupling of 50 kHz, providing an on/off ratio > 1000.

By incorporating tunable coupling with high coherence, our architecture provides a viable platform for both quantum computation and simulation. We applied this device to quantum simulation in a separate experiment where we demonstrated an interaction-driven topological phase transition [35]. Here, we focus on applications in quantum computation by implementing elementary logic gates. This architecture offers two distinct advantages: decoupling qubits for local single-qubit gates and dynamically tuning the interaction for fast two-qubit gates.

We characterize gate performance using a simplified form of randomized benchmarking [36,37], using a series of Pauli gates. These gates belong to a subset of the Clifford group and are generated with microwave pulses corresponding to Bloch sphere rotations of angle π and $\pi/2$ around the X and Y axes. From this set we randomly choose m gates and apply these to the qubit, including a final gate that ideally maps the qubit back into the ground state. The probability of finding the qubit in the ground state is called the sequence fidelity F_{seq}, which decays exponentially with the number of gates as $F_{\mathrm{seq}} = Ap^m + B$. Here, A, B, and p are fit parameters; A and B relate to state preparation and measurement. We are interested in the average error per gate r, determined through the relation $r = (1-p)(d-1)/d$, where $d = 2^{N_{\mathrm{qubits}}}$. We note that Pauli gates do not fully depolarize errors; hence, the extracted gate fidelities are only indicative.

The ability to isolate individual qubits for local operations is one advantage offered by a tunable coupling architecture. A metric to quantify this isolation is single-qubit gate fidelity $1-r$. For a baseline, we perform randomized benchmarking on the first qubit while the second qubit is far detuned and effectively decoupled. The sequence fidelity is plotted in Fig. 3(a) and displays the expected exponential decay with the number of random gates. Fitting the decay curve yields an average single-qubit gate fidelity of 99.86%. The two qubits are then placed on resonance with $g = 0$ and the measurement is repeated on both qubits; data for the first qubit are shown. Simultaneously operating the two qubits on resonance reduces the gate fidelity by less than 0.1%. The slightly increased error rate results from two sources: residual interqubit coupling, resulting from an imperfect choice of the zero coupling bias, and imperfect cancellation of microwave cross talk between control signals.

In Fig. 3(b), we repeat this measurement as a function of frequency separation of the two qubits, demonstrating that our architecture can resolve the frequency crowding issues from fixed coupling. The average error rate is plotted in Fig. 3(b) for both $g/2\pi = 0$ and 20 MHz. Even for this relatively weak interaction, the single-qubit gate fidelity undergoes a significant reduction for detunings less than 500 MHz. The ability to turn off the coupling g results in a nearly flat error rate, with an on-resonance value 2 orders of magnitude lower than for fixed coupling. We note the slight degradation near the qubit nonlinearity (220 MHz).

A concern in transmon design is the cross coupling of qubits. One solution is to use 3D devices where qubits are shielded in enclosing cavities [6]. Here we directly demonstrate that cross-coupling effects can be made small for planar integrated circuits, while still allowing for strong direct coupling for multiqubit operations.

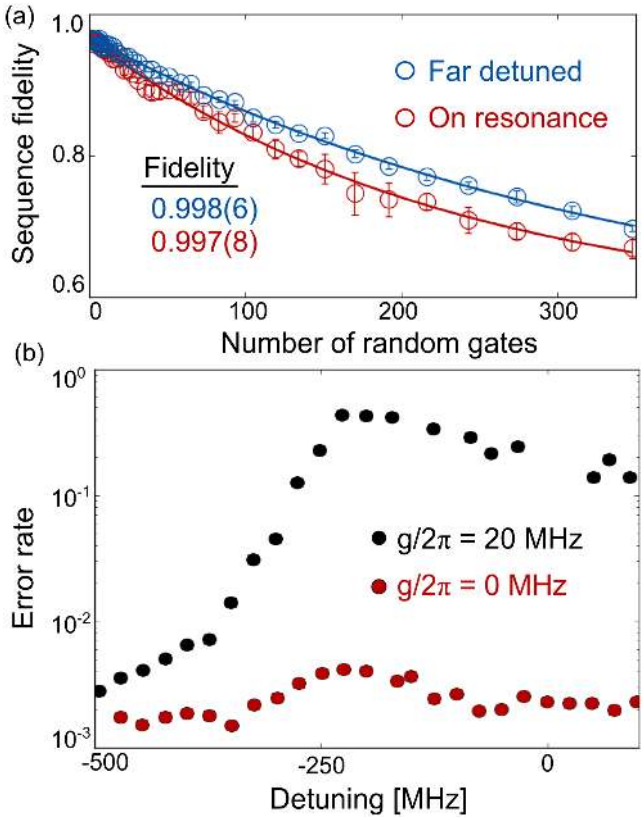

FIG. 3 (color online). Simultaneous single-qubit randomized benchmarking. (a) Raw benchmarking data for Q_1 when Q_2 is far detuned (blue) and on resonance (red) with random gates applied to both qubits. Operating the qubits on resonance degrades the gate performance by less than 0.1%. Lines are fits to a decaying exponential. (b) The average error rate for Q_1 as a function of detuning between the two qubits, shown for nominally 0 (red) and 20 MHz (black) coupling.

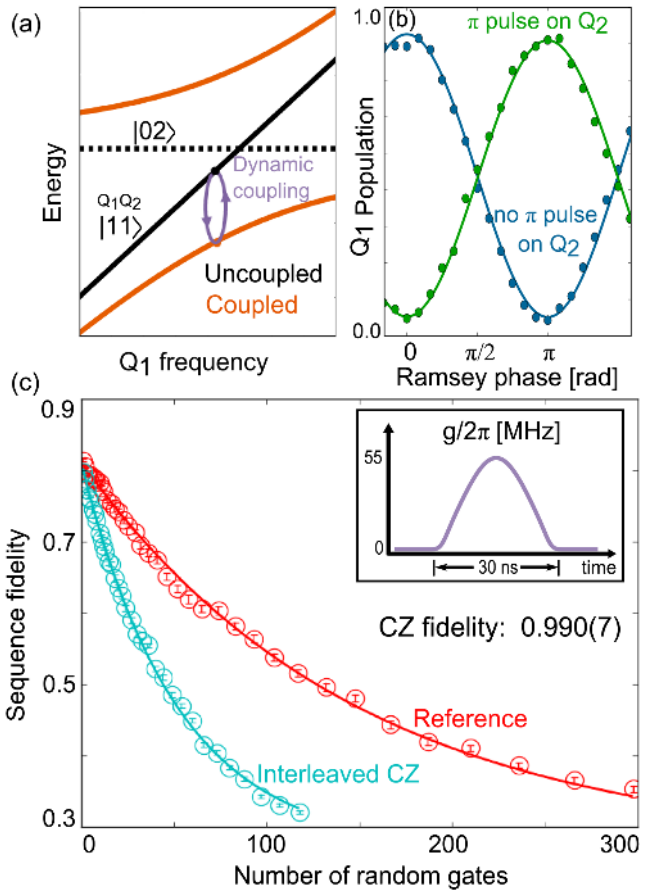

FIG. 4 (color online). (a) Energy level diagram, illustrating a CZ gate using tunable coupling. Black (orange) lines are the uncoupled (coupled) two-photon eigenenergies. As the coupling is tuned on and off (depicted in purple), the energy levels repel and the states accumulate a dynamic phase. (b) Ramsey data demonstrating zero phase shift for single-photon states and a π phase shift for the two-photon state. (c) Randomized benchmarking results for a CZ gate utilizing the pulse shape (inset). We achieve 99.07% fidelity with a 30 ns gate.

Control over the interaction strength with nanosecond resolution provides a unique tool to construct fast two-qubit gates. In Fig. 4(a) we illustrate the use of dynamical coupling to implement a fast CZ gate, with minimal nonadiabatic leakage errors. The straight lines correspond to the $|11\rangle$- and $|02\rangle$-state energies of the uncoupled system. Turning on the interaction pushes the energy levels apart, with the energies of the coupled system plotted as curved lines. Adiabatically turning on and off the coupling, as depicted with arrows, causes the $|11\rangle$ eigenstate to accumulate a dynamic phase. By calibrating the length of the interaction the phase shift can be set to π for a CZ gate.

In Fig. 4(b) we use a Ramsey measurement to verify that the gate produces the desired results. We first apply a $\pi/2$ pulse to Q_1, perform a CZ, apply a second $\pi/2$ pulse with varying phase, and then measure the Q_1 excited state probability. We then repeat the experiment with a π pulse applied to Q_2 and overlay the data. The solid lines are fits to cosine oscillations. As expected, the π phase shift is observed only when both qubits are excited; otherwise the phase accumulation is zero.

We extract the fidelity of this CZ gate using interleaved randomized benchmarking, where we insert a CZ between random single-qubit Pauli gates. A reference curve without the interleaved CZ is measured and plotted in Fig. 4(c) along with the interleaved sequence fidelity. Fitting these two curves allows us to extract an average CZ gate fidelity of 99.07%. The dominant error (~0.66%) comes from decoherence, measured by interleaved randomized benchmarking on the two qubit idle gate [27]. Surprisingly, despite the short gate time, the nonadiabatic error resulting from leakage to the $|02\rangle$ state is small (~0.25%), measured with the Ramsey error filter technique (see Ref. [27]) [30]. This results from using an optimized adiabatic trajectory based on a theory of optimal window functions [38]. The adiabatic trajectory used to vary the coupling strength is shown in the inset of Fig. 4(c).

High-fidelity gates have previously been demonstrated using Xmon qubits with fixed coupling [7]. We believe that gate fidelities can be further improved by instead employing tunable coupling. This will require incorporating lower loss materials, optimized capacitor geometry, and characterization using the full Clifford group; this is currently in progress.

This work was supported by the Office of the Director of National Intelligence (ODNI), Intelligence Advanced Research Projects Activity (IARPA), through the Army Research Office Grant No. W911NF-10-1-0334. C. N., P. R., and M. R. G. acknowledge support from the U.S. National Science Foundation under CDI Grant No. DMR-1029764. All statements of fact, opinion, or conclusions contained herein are those of the authors and should not be construed as representing the official views or policies of IARPA, the ODNI, or the U.S. Government. Devices were made at the University of California Santa Barbara Nanofabrication Facility, a part of the NSF-funded National Nanotechnology Infrastructure Network, and at the NanoStructures Cleanroom Facility.

Y. C., C. N., and P. R. contributed equally to this work.

*martinis@physics.ucsb.edu

†Present address: Google Inc., Santa Barbara, California, USA 93117.

[1] M. A. Nielsen and I. L. Chuang, *Quantum Computation and Quantum Information* (Cambridge University Press, Cambridge, England, 2000).
[2] J. Q. You and F. Nori, Phys. Today **58**, No. 11, 42 (2005).
[3] M. H. Devoret and R. J. Schoelkopf, Science **339**, 1169 (2013).
[4] A. Megrant *et al.*, Appl. Phys. Lett. **100**, 113510 (2012).
[5] R. Barends *et al.*, Phys. Rev. Lett. **111**, 080502 (2013).
[6] H. Paik *et al.*, Phys. Rev. Lett. **107**, 240501 (2011).
[7] R. Barends *et al.*, Nature (London) **508**, 500 (2014).
[8] J. M. Chow *et al.*, Nat. Commun. **5**, 4015 (2014).
[9] Y. P. Zhong, Z. L. Wang, J. M. Martinis, A. N. Cleland, A. N. Korotkov, and H. Wang, Nat. Commun. **5**, 3135 (2014).
[10] I. Buluta and F. Nori, Science **326**, 108 (2009).
[11] A. A. Houck, H. E. Türeci, and J. Koch, Nat. Phys. **8**, 292 (2012).
[12] M. R. Geller *et al.*, arXiv:1210.5260.
[13] A. Mezzacapo, L. Lamata, S. Filipp, and E. Solano, Phys. Rev. Lett. **113**, 050501 (2014).
[14] A. Polkovnikov, K. Sengupta, A. Silva, and M. Vengalattore, Rev. Mod. Phys. **83**, 863 (2011).
[15] P. Calabrese, F. H. L. Essler, and M. Fagotti, J. Stat. Mech. (2012) P07016.
[16] M. S. Allman, F. Altomare, J. D. Whittaker, K. Cicak, D. Li, A. Sirois, J. Strong, J. D. Teufel, and R. W. Simmonds, Phys. Rev. Lett. **104**, 177004 (2010).
[17] R. C. Bialczak *et al.*, Phys. Rev. Lett. **106**, 060501 (2011).
[18] R. Harris *et al.*, Phys. Rev. Lett. **98**, 177001 (2007).
[19] T. Hime, P. A. Reichardt, B. L. T. Plourde, T. L. Robertson, C.-E. Wu, A. V. Ustinov, and J. Clarke, Science **314**, 1427 (2006).
[20] A. O. Niskanen, K. Harrabi, F. Yoshihara, Y. Nakamura, S. Lloyd, and J. S. Tsai, Science **316**, 723 (2007).
[21] S. H. W. van der Ploeg, A. Izmalkov, A. M. van den Brink, U. Hüber, M. Grajcar, E. Il'ichev, H.-G. Meyer, and A. M. Zagoskin, Phys. Rev. Lett. **98**, 057004 (2007).
[22] S. J. Srinivasan, A. J. Hoffman, J. M. Gambetta, and A. A. Houck, Phys. Rev. Lett. **106**, 083601 (2011).
[23] A. Baust *et al.*, arXiv:1405.1969.
[24] A. Blais, A. Maassen van den Brink, and A. M. Zagoskin, Phys. Rev. Lett. **90**, 127901 (2003).
[25] Y.-x. Liu, L. F. Wei, J. S. Tsai, and F. Nori, Phys. Rev. Lett. **96**, 067003 (2006).
[26] R. A. Pinto, A. N. Korotkov, M. R. Geller, V. S. Shumeiko, and J. M. Martinis, Phys. Rev. B **82**, 104522 (2010).
[27] See Supplemental Material at http://link.aps.org/supplemental/10.1103/PhysRevLett.113.220502, which includes Refs. [28–31], for detailed discussion on the gmon control calibration, coherence, zero coupling, CONTROLLED-Z gate error characterization and transmon physics.
[28] J. M. Martinis, S. Nam, J. Aumentado, K. M. Lang, and C. Urbina, Phys. Rev. B **67**, 094510 (2003).
[29] D. Sank *et al.*, Phys. Rev. Lett. **109**, 067001 (2012).
[30] E. Lucero, M. Hofheinz, M. Ansmann, R. Bialczak, N. Katz, M. Neeley, A. O'Connell, H. Wang, A. Cleland, and J. Martinis, Phys. Rev. Lett. **100**, 247001 (2008).
[31] J. Koch, T. Yu, J. Gambetta, A. Houck, D. Schuster, J. Majer, A. Blais, M. Devoret, S. Girvin, and R. Schoelkopf, Phys. Rev. A **76**, 042319 (2007).
[32] M. R. Geller, E. Donate, Y. Chen, C. Neill, P. Roushan, J. M. Martinis, arXiv:1405.1915.
[33] M. Hofheinz *et al.*, Nature (London) **459**, 546 (2009).
[34] T. Yamamoto *et al.*, Phys. Rev. B **82**, 184515 (2010).
[35] P. Roushan *et al.*, Nature (London) **515**, 241 (2014).
[36] E. Knill, D. Leibfried, R. Reichle, J. Britton, R. B. Blakestad, J. D. Jost, C. Langer, R. Ozeri, S. Seidelin, and D. J. Wineland, Phys. Rev. A **77**, 012307 (2008).
[37] E. Magesan *et al.*, Phys. Rev. Lett. **109**, 080505 (2012).
[38] J. M. Martinis and M. R. Geller, Phys. Rev. A **90**, 022307 (2014).